https://doi.org/10.5194/egusphere-2026-4957
Preprint. Discussion started: 1 October 2026
© Author(s) 2026. CC BY 4.0 License.

Friction over gravitational forcing: Disentangling the controls of Hortonian overland flow and erosion through energy-centred process modelling

Doğa Yahşi[1]; Samuel Schroers[2]; Ulrike Scherer[3]; Núria Martínez-Carreras[4]; Erwin Zehe[1]

[1]Chair of Hydrology, Institute of Water and Environment, Karlsruhe Institute of Technology, Karlsruhe, 76131, Germany
[2]Fichtner, Stuttgart, 70191, Germany
[3]KIT Water Research/Division IV–Natural and Built Environment, Karlsruhe Institute of Technology, Karlsruhe, 76131, Germany
[4]Catchment and Eco-hydrology Research Group, Environmental Research and Innovation Department, Luxembourg Institute of Science and Technology, Belvaux, L-4422, Luxembourg

Correspondence to: Doğa Yahşi (doga.yahsi@kit.edu)

Abstract. This study investigates the coupled dynamics of Hortonian overland flow (HOF) and sediment transport observed during rainfall simulations at the plot scale using the process-based Catflow model with an energy centred approach. A hierarchical calibration strategy was applied to reproduce overland flow generation, flow velocities in sheet and rill domains and sediment detachment sequentially, allowing the dominant controls on HOF and erosion processes to be identified.

The results show that antecedent soil moisture and surface roughness are the primary controls on HOF generation, whereas rainfall intensity and slope had no significant effect within the investigated range. Increasing surface roughness reduced surface runoff and total sediment export, while simultaneously increasing the ratio between rill and sheet flow velocities, indicating enhanced flow concentration into preferential pathways. No clear relationship was observed between flow velocities and slope, demonstrating that overland flow dynamics are primarily limited by friction rather than gravitational forcing.

The model reproduced overland flow generation, flow partitioning and total eroded sediment with good consistency. The results indicate that sheet flow primarily governs sediment detachment and energy dissipation, whereas rills function as efficient sediment transport pathways. Increasing surface roughness promoted flow concentration into rills, where the greater hydraulic radius reduced relative frictional losses and enabled a more efficient conversion of potential into kinetic energy. Consequently, downslope kinetic energy transport became increasingly dominant within the rill domain, while the overall system remained friction dominated. This energetic interpretation links overland flow generation, flow organisation and erosion dynamics through the balance between energy input, dissipation and redistribution.

Overall, the study highlights the importance of frictional resistance as prime limitation of overland flow velocities, flow organisation and domain-specific flow representation for modelling infiltration-excess overland flow and erosion dynamics.

1 Introduction

Surface runoff, erosion and sediment redistribution play a pivotal role in terrestrial ecosystems as they directly influence water quality, soil biogeochemical cycles, soil functions and long-term evolution of landforms. While erosion leads to the onsite loss of fertile land, offsite impacts include flood damage in settlements, largely associated with flash floods, and the continuous deposition of sediments in reservoirs, which gradually impairs their storage capacity and functionality. Furthermore, suspended particles may carry substantial amounts of contaminants (pesticides, heavy metals) and nutrients (phosphorous) into surface water bodies impacting their water quality and threatening biodiversity and ecosystem health. A warmer climate will likely lead to more intense and frequent convective rainstorm due to Clausius-Clapeyron scaling, which will in turn trigger more coupled overland flow and erosion events (Trenberth et al. 2003, Nearing et al. 2004, Molnar et al. 2015, Martinkova and Kysely 2020). Furthermore, following prolonged dry periods, high-intensity convective storms may amplify surface runoff

https://doi.org/10.5194/egusphere-2026-4957
Preprint. Discussion started: 1 October 2026
© Author(s) 2026. CC BY 4.0 License.

production due to surface crusting and soil hydrophobicity. Hence, there is a strong need to better understand the factors that drive and limit these events.

Infiltration excess (Hortonian) overland flow (HOF) is an important response mechanism to high-intensity convective storms, especially in areas where soil frost affected or compacted soils and impermeable surfaces (Goodrich et al. 1995, Dingman 2015). HOF occurs when precipitation intensity exceeds soil infiltration capacity. Hillslope scale patterns of topography, soil types and their hydraulic characteristic and land use management (Knapen et al. 2007, Zhang et al. 2009, Scherer et al. 2012) are first-order controls of overland flow depth, velocity and connectivity (Richet et al. 2017). These characteristics, together with rainfall properties and antecedent soil moisture determine the shear stress applied to the soil surface and directly affect particle transport capacity, shaping the overland flow dynamics (Cammeraat 2004, Zehe and Blöschl 2004, Lesschen et al. 2009, Wainwright et al. 2011). These dynamics are rarely in steady-state conditions due to temporal variability of the precipitation events (Wainwright and Parsons 2002). Moreover, the flow encounters resistance due to the surface roughness from microtopography and vegetation, which creates spatial variability and affects the directions of overland flow pathways (Bergkamp 1998). The resistance caused by surface roughness can also change over time, due to erosion and modification of surface topography and infiltration characteristics (Puigdefabregas et al. 1999).

Soil surface roughness is thereby a dynamic soil property that changes with different erosion stages and help us to understand how microtopography relates to overland flow velocities, related energy dissipation and sediment detachment. Splash erosion and sheet erosion can decrease the soil surface roughness by flattening the surface and filling up the furrows, while rill and gully erosion might ultimately increase it (Zhao et al. 2014, Xinlan et al. 2015). Different tillage practices alter soil surface roughness to different degrees depending on the degree of additional complexity they introduce to the system. Conventional tillage methods create highly heterogeneous, multifractal microtopography that promote spatially concentrated flow and rill erosion (He et al. 2024).

Soil erosion results from non-linear interactions of three main processes: detachment, transport and sedimentation of soil particles. Particle detachment occurs when the shear stress generated by surface runoff and/or momentum transfer from rain splash exceeds the critical shear stress, representing the erosion resistance of the soil. This resistance is controlled by multiple factors such as soil texture, soil moisture, cohesion, surface preparation and the presence of roots (Govers et al. 2007, Knapen et al. 2007, Scherer et al. 2012). Concentrated overland flow often results in the erosive formation of small channels, rills and (ephemeral) gullies (Horton 1945, Emmet 1978, Kampf and Mirus 2013), that are active erosion areas with varying geometries over time, while dispersed sheet flow commonly triggers diffuse erosion. Naturally, both forms of erosion are associated with strongly different values of critical shear stress. Concentrated flow in rill networks increases the hydraulic radius relative to sheet flow, reducing specific energy dissipation while increasing flow velocity, boundary shear stress and stream power. As the shear stress generated by concentrated flow exceeds the critical threshold for detachment, erosion becomes localized and can develop into rills and gullies, whereas the lower shear stresses associated with dispersed sheet flow generally result in more diffuse erosion.

Hillslopes operate as thermodynamic systems that convert momentum and energy introduced by precipitation into the potential energy flux of overland flow, of which only a tiny fraction becomes kinetic energy flux of runoff and sediment, while the vast majority is dissipated through frictional resistance (see Figure 1) (Schroers et al. 2023). Spatially, potential energy flux peaks at intermediate slopes where mass accumulation outpaces elevation decline. Over evolutionary timescales, this peak migrates upslope and decreases in magnitude, reflecting the self-regulation of a system towards a slower morphological development, since available energy to perform work declines as hillslopes mature (Schroers et al. 2022). Furthermore, elevated kinetic energy within rills indicates that domain-specific flow partitioning may align with the maximization of power, implying an equitable distribution of kinetic energy fluxes across sheet and rill domains (Kleidon et al. 2013, Schroers et al. 2022).

https://doi.org/10.5194/egusphere-2026-4957
Preprint. Discussion started: 1 October 2026
© Author(s) 2026. CC BY 4.0 License.

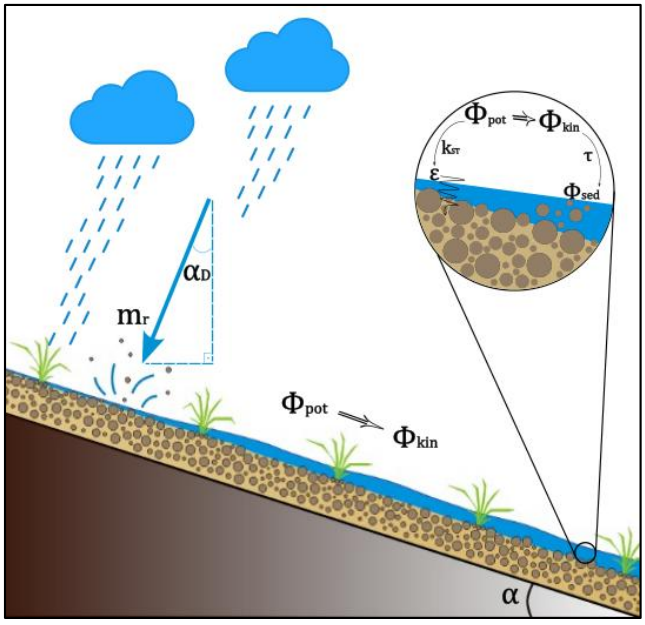

Figure 1 Conceptual schematic of energy-flux partitioning during rainfall-driven sediment transport where potential and kinetic energy fluxes are Φpot and Φkin (J s–1), momentum flux is mr (N m−2), the drop angle is αD (°), shear stress is τ (N m- 2), the Strickler coefficient is kST (m1/3 s-1), ε is dissipation flux and Φsed (J s–1) is the energy flux to the sediments.

Here we expand this energetic perspective, using a comprehensive dataset of 60 high-intensity rainfall simulations from the agricultural Weiherbach catchment, Germany (Gerlinger 1997). The main objectives of this study are:

1) to identify the primary controls on HOF flow generation, emphasizing the dominance of either gravitational forcing or friction,

2) to test the expanded "open book" approach flow partitioning into sheet and rill domains,

3) to explore energy conversions and energy transfer to the sediments, with a particular focus on potential and kinetic energy fluxes of overland flow.

Specifically, we investigate whether an expanded version of the open-book approach is feasible to reproduce the observed overland flow and its partitioning into two domains within the process-based model Catflow (Schroers et al. 2022). Using these verified models, we quantify stream power gains within rills to test out our hypothesis: flow partitions into sheet and rill domains to achieve an equal distribution of kinetic energy fluxes, enabling system self-optimization. We aim to identify the factors controlling where potential energy flux peaks along the hillslope and to evaluate whether the partitioning of energy fluxes aligns with the maximisation of power.

2 Methodology

2.1 Rainfall simulation experiments

The experiments were conducted to explore the formation of overland flow and the erodibility of the loess soils with a rainfall simulator (Figure 2) to ensure both realistic rainfall intensities (~35-65 mm h-1) and kinetic energies on plots of 2 m by 12 m in size (Gerlinger 199[illegible]). Sediment concentrations were determined from the overland flow samples collected during the experiments and rainfall simulation was stopped once overland flow and sediment concentration reached steady state. The different sites were characterized according to antecedent soil moisture, soil texture and organic content in the upper 10 cm (Scherer et al. 2012). Surface roughness was estimated from the falling limb of the observed hydrograph by using a kinematic

https://doi.org/10.5194/egusphere-2026-4957
Preprint. Discussion started: 1 October 2026
© Author(s) 2026. CC BY 4.0 License.

wave thereby varying the roughness coefficient iteratively until the best fitting predicted limb was achieved (Engman 1986, Govers et al. 2000). Rill flow velocities were estimated from upslope tracer injection based on the travel time of the tracer concentration peak to the plot outlet. Sheet flow velocities were subsequently back-calculated from measured total runoff rates and the estimated rill flow velocities using an overland flow mass balance. Further details on the experimental setup are provided by Gerlinger (1997), Seibert et al. (2011) and Scherer et al. (2012).

The experiments were carried out in the Weiherbach catchment, located in the agricultural Kraichgau region, northeast of Karlsruhe in Germany. The hilly landscape, the intensive agricultural use and the highly erodible loess soils result in a serious erosion problem in the region. Erosion is typically caused by high-intensity thunderstorms in late spring and summer, during which HOF dominates surface runoff generation (Schroers et al. 2022).

Figure 2 Transportable rainfall simulator (Scherer et al. 2012).

2.2 Analysis of experimental data

Initially, the data from all 60 rainfall-runoff experiments were analysed to characterize key hydrological and associated geomorphological responses of HOF. The main focus was on variables such as runoff coefficient, cumulative erosion and flow velocity, as well as their interrelations and relations to initial and boundary conditions.

Runoff coefficients were derived for all experiments from the available rainfall-runoff measurements. Relationships between runoff coefficients and key variables, slope, initial soil moisture content, rainfall intensity and roughness, were first explored using bivariate scatter plots. For the variables showing a significant correlation with runoff coefficients, a linear multivariate regression analysis was performed. Along similar lines, we analysed the distribution of overland flow between the sheet and the rill domains based on the corresponding velocity ratios. Finally, we explored the controls on total sediment yields by relating total eroded mass to the velocity ratios, roughness coefficients and total runoff.

2.3 The model Catflow

2.3.1 Catflow in a nutshell

Catflow was developed by Maurer (1997) and Zehe (1999) for simulation of the water balance, runoff generation, as well as solute (Klaus and Zehe 2011) and sediment transport (Scherer 2008, Schroers et al. 2022). The interaction of overland flow, preferential flow, soil moisture and erosion were proved to reproduce the observed dynamics successfully, from the plot scale transport to the small catchment scale rainfall runoff dynamics in different landscapes (Zehe et al. 2005, Klaus and Zehe 2011, Scherer et al. 2012, Loritz et al. 2017).

In the model Catflow, a catchment is subdivided into 2-D hillslope elements based on a digital elevation model (DEM), which might be connected to a river network. Hillslopes are strips of land along the gradient of the area between the highest point (hill crest) and the lowest point at the riverbank (hill foot). The third dimension is represented by a variable width, where each hillslope element is discretized using curvilinear orthogonal coordinates.

https://doi.org/10.5194/egusphere-2026-4957
Preprint. Discussion started: 1 October 2026
© Author(s) 2026. CC BY 4.0 License.

The soil water dynamics are modelled using the 2-D Richard's equation, which is solved numerically by a mass conservative Picard iteration scheme. Soil hydraulic properties such as the soil hydraulic conductivity as a function of the relative saturation and the soil retention function and the soil moisture as a function of the matric potential are characterized by using the van Genuchten-Mualem and the Peters–Durner–Iden (PDI) (Peters 2014) models.

Flow through macropores can be simulated either through their representation as connected elements with neglectable retention or through enhancing infiltrability due to activated macropore flow. If the relative saturation at a grid point at the solid surface exceeds a certain experimentally determined threshold, the hydraulic conductivity is enlarged by using a macroporosity factor f_{mak} (-). As this approach is well suited for predicting rainfall–runoff dynamics (Zehe et al. 2005, Schroers et al. 2022), we adopt it in our model study.

2.3.2 Overland flow and erosion in Catflow

The mass and momentum balance of overland flow is simulated in Catflow using the diffusive wave equation (DSW), which is a simplified form of the 1-D shallow water equations. DSW assumes that the horizontal momentum can be linked to the velocity by an empirical relation. Thus, the DSW reduces to a scalar equation that resembles nonlinear diffusion (Zehe et al. 2001, Collier et al. 2011), which can be solved numerically by using an explicit upstreaming scheme (Scherer 2008). In Catflow, the empirical Manning-Strickler formula is adopted for this link (Eq. (A *2*)).

Inspired by Wooding (1965), a hillslope surface similar to an open book catchment has been conceptualized by Schroers et al. (2022) to incorporate the rill domain into the model, providing a dynamic interaction between rill and sheet flow. The representation of both domains is seen in Figure 3. In this approach, the link between sheet and rill flow is established by a flow accumulation coefficient (see Eq. (A 3)). Here, we expand the open book approach by introducing a separate rill roughness value, as the rill and the sheet domain have fundamentally different dynamics. That is, sheet flow is shallow and strongly influenced by microtopography and vegetation, while rill flow is deeper, more turbulent and experiences much lower resistance due to a greater hydraulic radius. Thus, separate roughness values were integrated to the model in this study, to ensure realistic flow rates and erosion estimates.

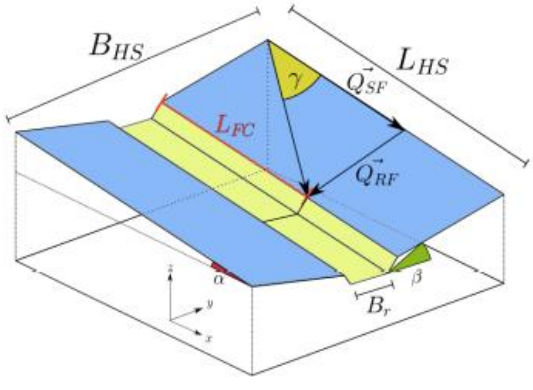

Figure 3 Representation of overland flow domains in Catflow as open book hillslope: Sheet flow domain (blue area) and rill flow domain (green area), where rill domain width is Br (m), hillslope width is B_{HS} (m), downslope length is L_{HS} (m), flow path length is L_{CF} (m), sheet flow and rill flow are Q_{SF} and Q_{RF} (m^3 s^{-1}), the angle between rill and sheet domains is γ (rad), the hillslope gradient is α (rad) and the secondary flow accumulation gradient is β (rad) (Schroers et al. 2022).

Note that the calculation of the potential energy flux in either domain is straight forward with $\phi_{pot} = \rho Q g z$ (J s^{-1}), where ρ (kg m^{-3}) is the density of water, Q (m^3 s^{-1}) is overland flow, g (m s^{-2}) is gravitational acceleration and z (m) is surface elevation. Additionally, the power of overland flow corresponds to the kinetic energy flux $\phi_{kin} = \frac{1}{2}\rho Q v^2$ (J s^{-1}), and replacing the density of water with the sediment concentration in the formula gives the power of sediment flux. Total work performed by overland flow (J m^{-1}) can be calculated by taking the integral of total power over time.

https://doi.org/10.5194/egusphere-2026-4957
Preprint. Discussion started: 1 October 2026
© Author(s) 2026. CC BY 4.0 License.

Erosion processes are based on the sediment continuity equation in Catflow, which is constructed around the principle of conservation of mass, forming the basis for the mathematical description of three main erosion processes: detachment, transport and deposition of particles. Due to the very shallow overland flow depth, it can be assumed that the advective component dominates the sediment flux (Bennett 1974). The steady-state sediment continuity equation is given in Eq. 1 (Scherer 2008). In this formulation, e_{pot} (kg m^{-2} s^{-1}) represents the potential detachment rate, S_{dep} (kg m^{-2} s^{-1}) is the deposition rate and q_s (kg (ms)$^{-1}$) denotes the width-specific solid mass flux. The equation assumes quasi-steady-state conditions, meaning that erosion and deposition rates remain approximately constant over time, so that the spatial change in sediment flux, $\frac{\partial q_s}{\partial x}$ (kg m^{-2} s^{-1}), balances the difference between detachment and deposition.

$$e_{pot} - S_{dep} = \frac{\partial q_s}{\partial x} \qquad \textbf{Eq. 1}$$

Further details on the process representations and equations can be found in the appendix section of this study, as well as Scherer (2008) and Schroers et al. (2022).

2.3.3 Model setup, sensitivity and calibration

For the modelling study, we selected 30 of the rainfall experiments that reached steady-state in either overland-flow rates or sediment concentrations at the outlet. We then calibrated the Catflow model using a hierarchical approach to reproduce observed overland-flow amounts and velocities in both the sheet and rill domains, as well as the observed total erosion.

At a first step, each experimental plot was discretised using a two-dimensional grid with 21 nodes in the lateral direction and 29 nodes in the vertical direction. In the vertical profile, the upper 10 cm were discretised in 1 cm increments, while the lower 90 cm were represented with a coarser resolution of 5 cm increments down to a total depth of 1 m. Soil hydraulic properties were assigned to the model domains using parameter values derived for the respective soils, as summarized in Table A 2. The model was driven by block rainfall events defined by the measured rainfall intensity and duration of each experiment, implemented through atmospheric boundary conditions at the surface. The lower boundary condition was defined as gravity flow, while the left and the right boundaries were no flow.

Model calibration was performed for the selected experiments using a three-level hierarchical approach aimed at first reproducing (i) overland flow generation, then (ii) flow velocities in the sheet and rill domains and finally (iii) and total erosion. The purpose of the first step was to reproduce the observed hydrograph and ensure the mass balance of overland flow. To achieve this, the macroporosity factor f_{mak} and, if necessary, the initial soil moisture were calibrated to match the amount and initiation time of overland flow. Macroporosity factor was calibrated since it was not measured on the rainfall simulation plots, while initial soil moisture was measured only at a single point in the top 15 cm, which may not have been representative of the entire study area and can therefore be reasonably adjusted.

After reproducing the hydrograph, the model was calibrated against the observed flow velocities. Because rill flow velocities were measured directly and were therefore considered more reliable, they were calibrated first. Sensitivity analysis showed that simulated rill flow velocities were considerably more sensitive to the flow accumulation coefficient than to the rill domain roughness. Consequently, calibration primarily focused on adjusting the flow accumulation coefficient, while only minor modifications to the rill domain roughness were made where necessary to improve agreement with the observations. Subsequently, the sheet domain roughness was adjusted to reproduce the observed sheet flow velocities. In the third step, the model was calibrated for the total detached sediment amount by varying the erosion resistance f_{crit}. The parameter range was defined based on laboratory findings and direct measurements reported by Scherer et al. (2012), with a precision of two decimal places.

Model performance was evaluated using the Nash–Sutcliffe efficiency coefficient based on total observed runoff and the total eroded mass. Uncertainty was represented using a relative error approach. Simulation results are shown with ±10% uncertainty

https://doi.org/10.5194/egusphere-2026-4957
Preprint. Discussion started: 1 October 2026
© Author(s) 2026. CC BY 4.0 License.

bands, reflecting potential variability in model predictions, while observational data include ±10% error bars to account for measurement uncertainty.

The final setups were used to quantify the potential and kinetic energy fluxes in both flow domains to analyse HOF formation from an energetic perspective, where the partitioning of energy fluxes into two domains and the related controls are of key interest.

3 Results

3.1 Analysis of experimental data

3.1.1 Runoff coefficients and multivariate linear regression analysis

Runoff coefficients demonstrated an apparent increase with increasing soil moisture and a strong decline with increasing roughness. The effect of rainfall intensity could not be assessed because only two rainfall intensity levels were included in the experiments. There was no apparent relationship between runoff coefficients and slope.

The coefficient of determination R^2 was approximately 0.50, indicating that soil moisture and roughness together explained about half of the observed variation in runoff coefficient (see Table A 1). Additionally, the probability value for the overall f-test was smaller than 0.05, which indicates that the analyses were statistically significant. The same was valid for the individual p-values of the variables. In other words, both soil moisture and roughness were found to be good linear predictors for runoff coefficient in these experiments.

3.1.2 Flow velocities

The ratio of rill flow velocity to sheet flow velocity as well as the individual domain velocities, showed no relationship with slope. This ratio showed a strong decrease with decreasing experimental surface roughness values (i.e., increasing Strickler coefficient), as shown in Figure 4 (a).

3.1.3 The total eroded material

The total eroded material mass slightly declined with both increasing ratio of steady-state rill velocities to sheet velocities (R^2=0.18) and increasing roughness coefficients (R^2=0.27). There was an apparent increase observed in the total eroded mass with increasing total runoff (Figure 4 (b)). The regression analysis revealed that the total eroded mass increased with approximately the square of overland flow, which is a proxy of the related kinetic energy.

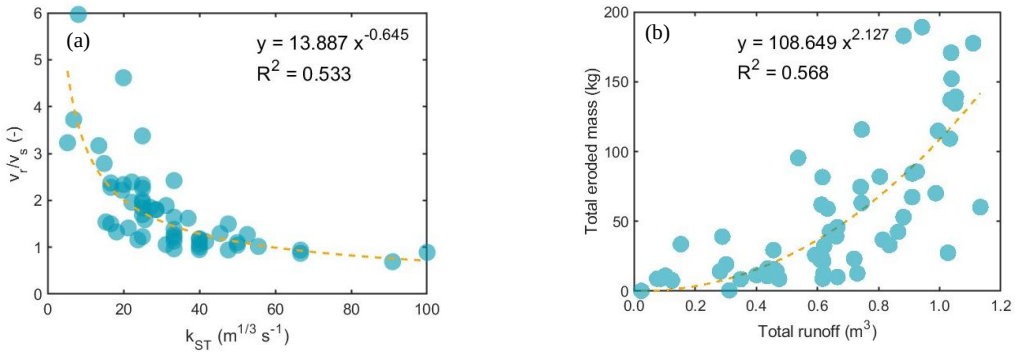

Figure 4 Evaluation of controls on flow partitioning and sediment production and: (a) Rill-sheet velocity ratio vs. experimental Strickler roughness values (power fit), (b) total eroded mass vs. total runoff (power fit) for 60 experiments.

https://doi.org/10.5194/egusphere-2026-4957
Preprint. Discussion started: 1 October 2026
© Author(s) 2026. CC BY 4.0 License.

3.1. Model results

Overall, the model performed well in estimating total overland flow across all 30 calibrated experimental setups. For some setups, total overland flow was overestimated, whereas only a few cases were underestimated (Figure 8 (b)).

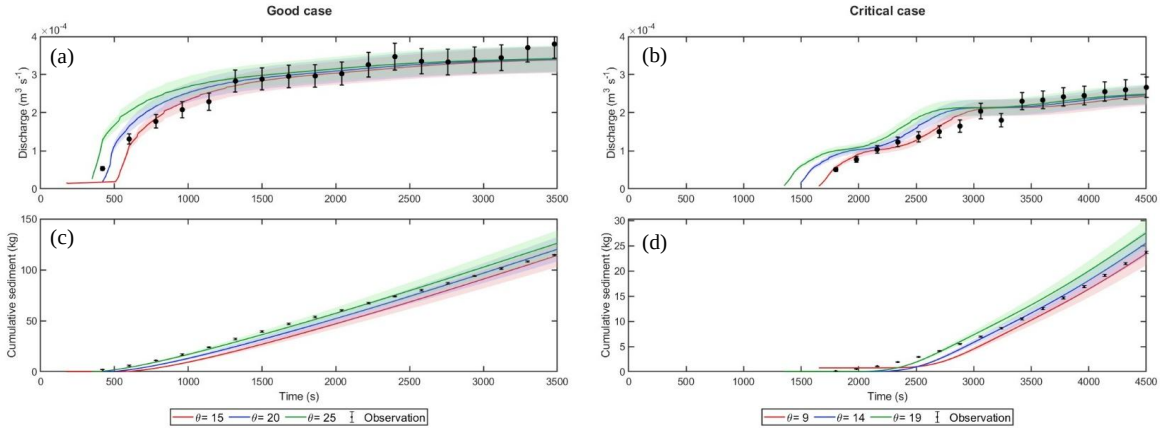

Figure 5 Model predictions and 10% error bands of (a, c) good case and (b, d) critical case simulations with different initial soil moisture values.

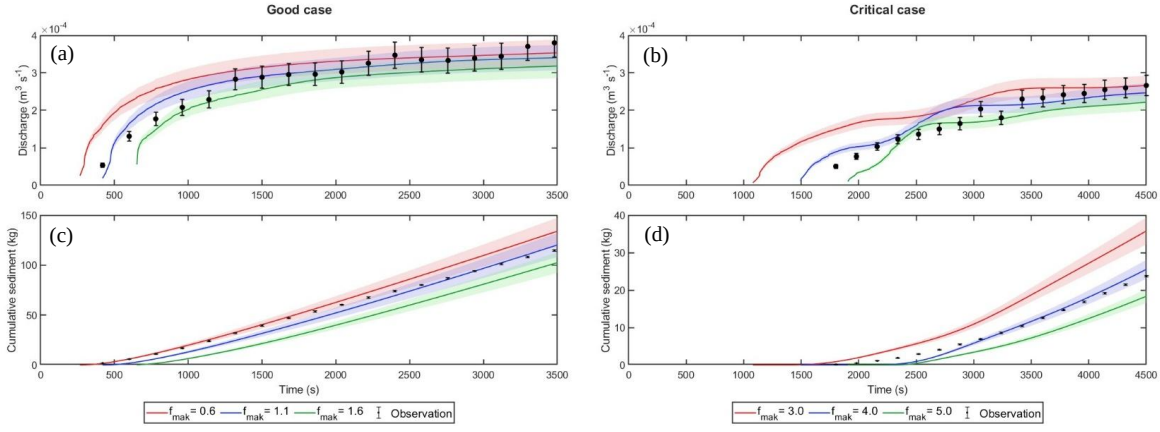

Figure 6 Model predictions and 10% error bands of (a, c) good case and (b, d) critical case simulations with different macroporosity factors.

The effects of different initial soil moisture values and macroporosity factors are shown in Figure 5 and Figure 6, respectively, for the exemplary good case (experiment 21) and critical case (experiment 30) setups (see Table A 3). The initiation of overland flow occurs earlier with increasing initial soil moisture and decreasing macroporosity. The total overland flow volume increases with higher soil moisture and decreases with higher macroporosity, although the simulation results converge toward the end of the simulation, particularly in the good case. Under low antecedent soil moisture conditions, the hydrograph in the critical case becomes unstable.

The partitioning of overland flow volume into two domains was performed to match the observed steady-state rill and sheet flow velocities by adjusting the flow accumulation coefficient c_{FC} with a precision of three decimal places. In addition, different Strickler coefficients were assigned to each domain for further calibration until the residual values were reduced to less than 1% of observed velocities. This procedure resulted in a one-to-one agreement between the simulated and observed velocities in both domains (see Figure A 1). The ratio of simulated rill and sheet domain discharge was plotted against the ratio of observed rill and sheet domain velocities as seen in Figure 7. The analysis indicates that the simulated flow partitioning

https://doi.org/10.5194/egusphere-2026-4957
Preprint. Discussion started: 1 October 2026
© Author(s) 2026. CC BY 4.0 License.

accounts for roughly 95% of the variance in the measured velocity ratios. The relationship reveals an increasing concave down trend: as the ratio of rill-to-sheet discharge increases, the corresponding increase in the velocity ratio eventually tapers off.

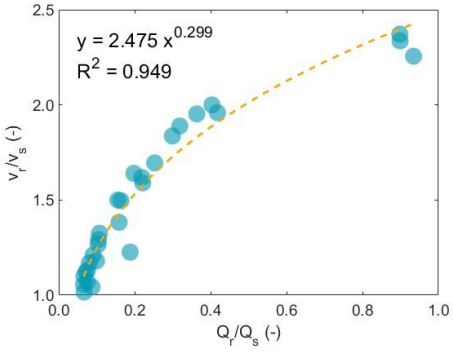

Figure 7 Rill-sheet velocity ratio vs. simulated rill-sheet discharge ratio (power fit) for 30 calibrated experiments.

The model reproduced the total eroded sediment amounts well with only varying f_{crit}, while for some of the 30 experiments overestimations were observed in the simulations (Figure 8 (a)).

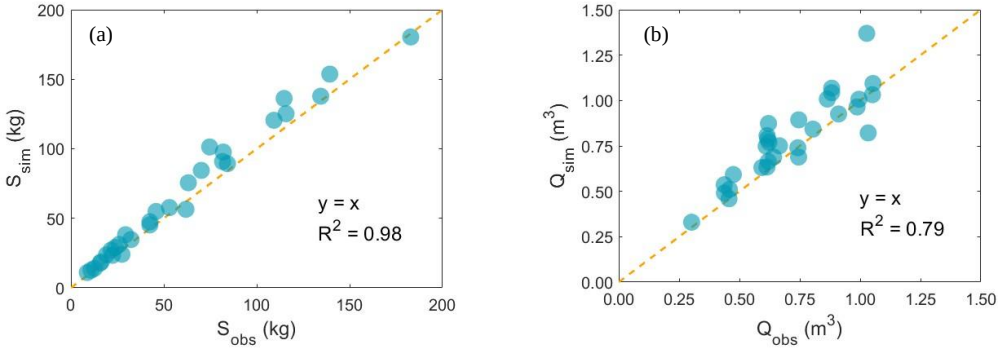

Figure 8 Evaluation of model accuracy: (a) Simulated vs. observed erosion, (b) simulated vs. observed discharge for 30 calibrated experiments.

3.1.5 Energy balance of surface runoff

The potential and kinetic energy fluxes in both domains for 30 calibrated experiments and their spatial distribution is shown in Figure 9. For both domains, potential energy represents the dominant share of total energy and increases throughout the slope at a decreasing rate, whereas kinetic energy remains three orders of magnitude smaller, but displays an accelerating growth downslope. The potential energy fluxes are higher in the sheet-flow domain due to presence of greater water mass, whereas the kinetic energy fluxes become more similar and partially greater in the rill domain toward the end of the plot.

The local maxima of potential energy flux results from the trade-off relationship of decline in geopotential and increase in water mass. There was a reasonable correspondence between the local maxima of potential energy flux within the rill domain and the flow accumulation coefficients. This location shifted further downslope with increasing flow accumulation coefficients (Figure 10) and the more downslope occurrence of maxima was associated with higher energy flux and flow velocity in the rill domain.

https://doi.org/10.5194/egusphere-2026-4957
Preprint. Discussion started: 1 October 2026
© Author(s) 2026. CC BY 4.0 License.

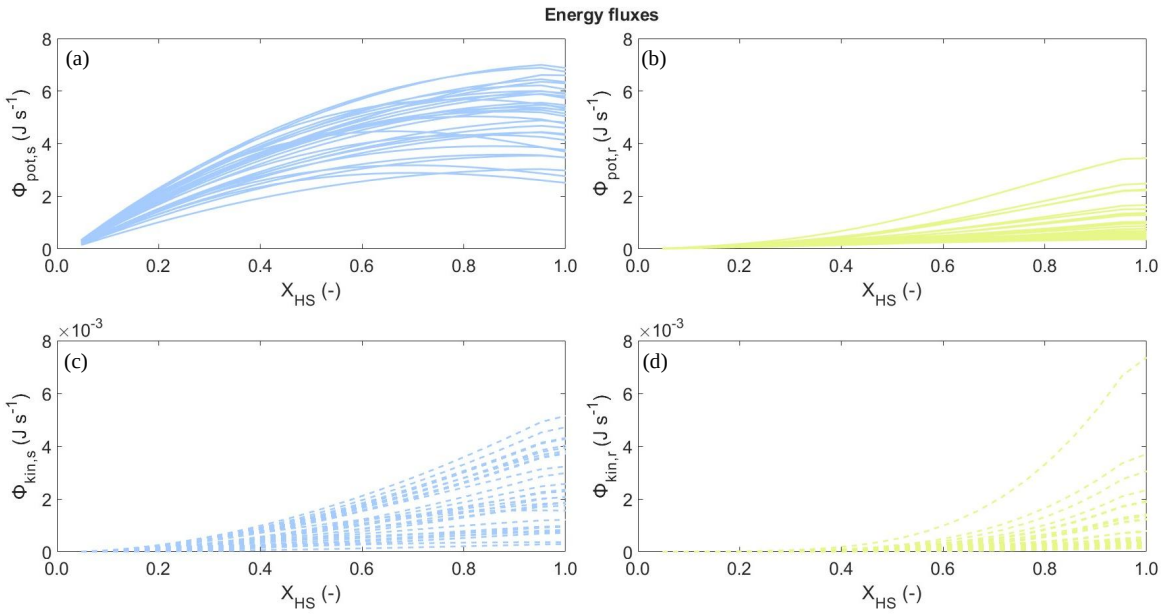

Figure 9 Potential (a,b) and kinetic (c,d) energy fluxes in the sheet (a,c) and the rill (b,d) domain for 30 calibrated experiments calculated with the simulation results, where X_{HS} (-) is the normalized hillslope length.

The regression analysis between total eroded mass and total work done across all experiments showed that total eroded mass increased with increasing work (Figure 11). Results are consistent with Figure 4 (b), with total work performed by stream explaining approximately 5% more variance than total runoff volume. Separate analyses for the sheet and rill domains indicated that the sheet domain exhibited a similar relationship, whereas no clear relationship was observed for the rill domain between total eroded mass and stream power available to perform work. The ratio of the total work performed by the rill domain to that of the sheet domain decreased slightly with back calculated experimental roughness values, with the sheet domain predominantly accounting for a greater share of the work (Figure A 2).

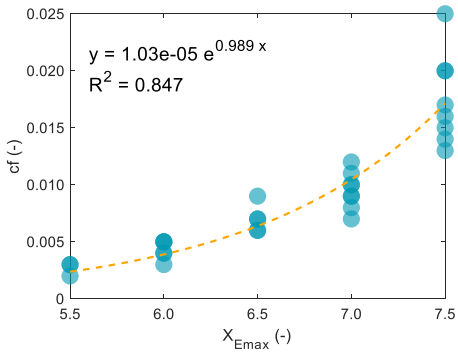

Figure 10 Flow accumulation coefficient vs. location of potential energy flux maxima in the rill domain (exponential fit) for 30 calibrated experiments, where X_{Emax} (-) is the normalized location relative to the total hillslope length.

https://doi.org/10.5194/egusphere-2026-4957
Preprint. Discussion started: 1 October 2026
© Author(s) 2026. CC BY 4.0 License.

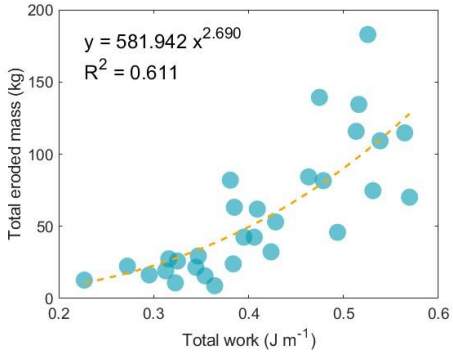

Figure 11 Total eroded mass vs. total work (power fit) for 30 calibrated experiments.

4 Discussion

Our study demonstrates that the coupled dynamics of overland flow generation, flow partitioning and sediment transport in rainfall-driven erosion on plot scale can be reproduced with good consistency using a hierarchical calibration strategy conducted with the Catflow model. Beyond overall model performance, the results provide insight into the relative importance of hydrological state variables, surface characteristics and flow organization in controlling HOF and associated erosion processes.

The statical analysis performed for runoff coefficients clearly indicates that antecedent soil moisture and surface roughness are the dominant controls on overland flow generation across the experimental setups, while rainfall intensity and slope do not emerge as significant predictors within the tested range. The strong influence of initial soil moisture is consistent with established hydrological understanding, as wetter soils exhibit reduced infiltration capacity and storage potential, thereby promoting earlier surface runoff initiation and higher runoff volumes (Western et al. 2002, Penna et al. 2011). The necessity to adjust initial soil moisture during calibration, despite available measurements, further highlights the limitations of point-scale observations in representing spatial heterogeneity of soil conditions at the plot scale.

Surface roughness has a similarly strong but inverse control on overland flow generation. Increased roughness enhances depression storage and flow resistance, thereby increasing infiltration and delaying flow connectivity and reducing effective runoff (Giménez and Govers 2001, Darboux et al. 2002). The absence of a clear relationship between rainfall intensity and runoff coefficient suggests that, under the experimental conditions, rainfall inputs were overall sufficient to exceed the infiltration capacity, shifting the system toward a state where internal soil and surface properties dominate runoff response. The linear regression analysis revealed no significant relationship between runoff coefficients and slope, suggesting that slope was not a dominant control on overland flow generation under the experimental conditions.

A central finding of this study is the systematic increase in the ratio of rill to sheet flow velocities with increasing roughness. This indicates that, as resistance increases, flow becomes increasingly concentrated in preferential pathways. In other words, water follows the path of least resistance, leading to enhanced flow concentration and more efficient energy use within rills, which is consistent with conceptual and experimental work on flow concentration and microtopographic control (Dunne et al. 1991, Govers et al. 2007).

At the same time, no relationship was found between the velocity ratio and slope. This is an important finding, as it demonstrates that overland flow velocities are not limited by the available potential energy but instead limited by friction. Although gravitational forcing provides the energy input, this energy is largely dissipated by surface resistance before it can be converted into kinetic energy, which is the reported behaviour for shallow water overland flow under rough conditions (Abrahams et al. 1986, Abrahams et al. 1994, Nearing et al. 1997, Niu et al. 2025). As a result, increases in slope do not

https://doi.org/10.5194/egusphere-2026-4957
Preprint. Discussion started: 1 October 2026
© Author(s) 2026. CC BY 4.0 License.

translate into proportional increases in flow velocity. This frictional limitation explains the observed flow reorganisation: as roughness increases and energy dissipation intensifies, flow concentrates into rills where resistance is lower due to larger hydraulic radius and conversion from potential to kinetic energy takes place more efficiently. Since kinetic energy scales with the square of velocity, this concentration leads to a disproportionate increase in energetic efficiency within the rill, even though the overall system remains friction-dominated (Nearing et al. 1997).

The calibration results support this interpretation (see Table A 3), showing that rill flow velocities are primarily controlled by the flow accumulation coefficient, i.e. by flow convergence, rather than by local roughness. In contrast, sheet flow velocities remain directly controlled by surface resistance. This distinction highlights the importance of explicitly representing flow connectivity and spatial erosion modelling (Takken et al. 1998, Reaney et al. 2014).

Total eroded mass slightly declines with increasing roughness, which can be attributed to reduced stream power and limited transfer of kinetic energy to the soil surface. Higher friction dissipates energy within the flow, leaving less energy available for particle detachment, in agreement with established stream power concepts (Bagnold 1966, Nearing et al. 1997). In addition, total eroded mass slightly decreases with increasing steady state rill-to-sheet velocity ratios. This may indicate that sediment detachment predominantly occurs in the sheet flow domain, where energy transfer to the sediments is distributed over a larger surface area. As flow becomes increasingly concentrated in rills, the active area of detachment decreases, even though transport capacity within rills may increase. Thus, we suggest that roles of the two domains reflect a functional differentiation: sheet flow acts as the primary zone of energy dissipation through particle detachment, whereas rills primarily transport sediment and perform mechanical work on already detached material. The positive relationship between total runoff and eroded mass remains consistent with this interpretation, as greater water flux increases the overall energy available to drive both detachment and transport processes (Meyer-Peter and Müller 1948, Foster 1982).

The hierarchical calibration strategy proved essential for resolving the coupled controls on hydrology and erosion. By sequentially constraining overland flow generation, flow velocities and soil detachment, the approach reduces parameter ambiguity and ensures that each process is represented based on its dominant controls. This is in line with multi-objective and stepwise calibration strategies recommended in hydrological modelling (Gupta et al. 1998, Vrugt et al. 2003).

The first calibration step highlighted the sensitivity of overland flow generation to macroporosity and initial soil moisture, emphasizing the role of soil structure and preferential flow pathways (Beven and Germann 1982). Although the model performed well in representing the overland flow formation, the observed insatiability of hydrographs under low antecedent soil moisture conditions points to the limitations in representing infiltration dynamics under drier conditions, suggesting that further refinement of soil hydraulic parametrisation may improve model robustness. This could potentially also include a switch from van Genuchten to the PDI soil water retention model, as the latter performs better at dry conditions.

The second calibration step demonstrated that an accurate representation of flow partitioning requires explicit consideration of both flow accumulation and domain-specific roughness. The primary control is the flow accumulation into the rill domain, as it directly affects the water volume within the domain, which influences flow depth and velocity. While calibrating the domain-specific roughness values alone was not sufficient to fully reproduce the observed velocities, it improved the agreement between simulated and observed velocities. Moreover, the ratio of observed rill-to-sheet velocities revealed a clear relationship to the ratio of simulated rill-to-sheet runoff, proving the representation of domain-specific flow partitioning with open book approach captures the actual kinetic dynamics observed during the experiments. The increasing concave down trend reflects how friction constrains velocity gains even as relative volume in the rill domain increases.

The final calibration step confirmed that sediment dynamics can be reproduced once hydrological and hydraulic conditions are appropriately constrained. The successful reproduction of total eroded sediment using a single erosion resistance parameter further indicates that, once flow dynamics and partitioning are correctly captured, sediment response can be effectively constrained. Erosion resistance values were comparable to critical shear stress values reported for sheet erosion initiation and the lower range of rill erosion initiation (Gilley et al. 1993, Poesen et al. 2003, Foltz et al. 2008, Ahmad et al. 2011, Winterwerp

https://doi.org/10.5194/egusphere-2026-4957
Preprint. Discussion started: 1 October 2026
© Author(s) 2026. CC BY 4.0 License.

et al. 2012, Li et al. 2024), suggesting that sheet erosion is the dominant erosion mechanism in the study area. Slight overestimation of eroded material in some cases suggests that additional processes such as deposition or selective transport may locally influence sediment dynamics.

The energetic perspective provides a unifying framework by linking overland flow generation, flow velocities, flow partitioning and erosion dynamics through a common control: the balance between potential energy input and frictional energy dissipation. While potential energy of runoff represents the dominant energy input, its conversion into kinetic energy is strongly limited by friction. As a result, the system is characterised by high energy dissipation and limited kinetic energy availability, particularly in the sheet flow domain. This perspective is consistent with energy-based interpretations of erosion processes (Bagnold 1966, Hergarten 2020).

The increase in kinetic energy flux (power) downslope especially in rill flow, reflects the progressive concentration of flow and reduction of relative frictional losses within preferential pathways. However, this increase does not contradict the overall friction-dominated regime; rather, it illustrates how the system reorganises to maintain flow under increasing resistance. The spatial patterns of energy fluxes confirm that rills act as zones of concentrated energy transfer, whereas sheet flow represents a dissipation domain. Moreover, the higher potential energy fluxes in the sheet-flow domain and the convergence of kinetic fluxes toward the end of the experimental plot suggest the development of a maximum power configuration. This perspective explains both the observed flow organisation and the reduction in total erosion with increasing roughness, linking hydrodynamics and sediment processes through a consistent energetic interpretation. Contrary to our hypothesis that flow divides to achieve an equal distribution of kinetic energy, total kinetic energy fluxes in the rill domain were mostly lower than in the sheet domain. This highlights a limitation in using fluid kinetic energy alone to measure system self-organization. First, our analysis focused on water movement while leaving out the power in the sediment flux, which consume a major share of energy, especially in rills. Second, although steady-state flow was assumed, experimental setups were often transient and may not have reached a true balanced state. Consequently, the system may not have had enough time or distance to fully organize toward the theoretical energy balance predicted by maximum power principles.

The spatial analysis of energy fluxes further supports the interpretation of a friction-dominated dynamically reorganising flow system. The downslope shift of potential energy flux maxima with increasing flow accumulation coefficients (also with increasing flow velocity) demonstrates that increasing flow convergence enhances the mass and energy flux in the rill domain and promotes more efficient use of energy along preferential pathways. This behaviour highlights the role of rills as zones of concentrated energy transfer. While long-term landscape evolution drives a progressive upslope migration of energy peaks as hillslopes mature and flatten (Schroers et al. 2022), our event-scale spatial analysis demonstrates that active hydraulic reorganisation within individual events concentrates energy flux downslope along evolving rill pathways.

The regression analysis between total eroded mass and total work done further highlights the importance of energetic controls on erosion dynamics, as well as demonstrating that sediment detachment depends on the flow's available power to perform work. While a clear positive relationship was observed for the overall system and the sheet flow domain, no such relationship emerged in the rill domain. This supports the interpretation that sheet flow primarily governs sediment detachment and energy dissipation, whereas rills mainly act as sediment transport pathways controlled by local hydraulic conditions and flow concentration. Together, these findings demonstrate how flow organisation redistributes energy and differentiates the functional roles of both domains.

The findings of this study challenge slope-centric interpretations of overland flow and erosion by demonstrating that, under the investigated conditions, friction is the primary limiting factor controlling velocities, energy flux and erosion efficiency. This has important implications for both experimental analysis and model development. Furthermore, the results suggest that energy-based approaches, when combined with domain-specific flow representation, provide a powerful framework for understanding process interactions. By focusing on energy dissipation and redistribution rather than solely on energy input, such an approach can better capture the emergent behaviour of complex flow systems.

https://doi.org/10.5194/egusphere-2026-4957
Preprint. Discussion started: 1 October 2026
© Author(s) 2026. CC BY 4.0 License.

5 Conclusion

The coupled processes overland flow generation, flow partitioning and sediment transport during HOF driven erosion at the plot scale were reproduced consistently using the Catflow model combined with a hierarchical calibration strategy. Prior analysis of the experimental data informed the selection of the calibration parameters. By sequentially constraining overland flow generation, the partitioning of flow mass between sheet and rill domains and finally sediment detachment, the hierarchical calibration approach reduced parameter ambiguity and enabled a process-oriented interpretation of erosion dynamics.

The analysis of experimental data showed that antecedent soil moisture and surface roughness are dominant controls on runoff generation under the investigated conditions, whereas rainfall intensity and slope did not significantly influence runoff coefficients in the tested range. More saturated soils promoted faster runoff initiation and larger runoff volumes due to reduced infiltration capacity, while increasing surface roughness enhanced depression storage, infiltration and flow resistance, thereby reduced effective runoff.

A key finding of this study is that the ratio of rill flow velocities to sheet flow velocities increase with increasing roughness, indicating progressive flow concentration into preferential pathways. At the same time, the absence of a relationship between velocity ratios and slope demonstrates that overland flow velocities are primarily limited by friction rather than controlled by gravitational forcing alone. Although slope provides the potential energy input, much of this energy is dissipated by surface resistance before being converted into kinetic energy. As roughness increases, the system reorganises dynamically by concentrating flow into rills where hydraulic resistance is lower and energy flux becomes more efficient.

The erosion response reflects the same energetic controls. Total eroded mass decreases with increasing roughness and increasing rill-to-sheet velocity ratios, indicating that sediment detachment is mainly associated with the sheet flow domain, where energy dissipation occurs across a larger surface area. In contrast, rills primarily act as transport pathways for already detached sediment. The positive relationship between runoff volume and eroded sediment confirms that the total water flux controls the overall energy available for detachment and transport.

Overall, the findings show that frictional resistance and flow organisation are the primary controls on velocities, energy flux and erosion efficiency under the investigated conditions, and challenge slope-centric interpretations of overland flow and erosion dynamics. The study highlights the importance of explicitly representing flow connectivity, domain-specific hydraulics and energy dissipation in overland flow and erosion modelling.

Appendix A

Representation of overland flow and erosion processes in Catflow:

The governing mass balance equation is given in Eq. (A 1), where *t* (s) is time, *x* (m) is lateral distance along the hillslope, *h* (m) is overland flow depth and *v* (m s^{-1}) is overland flow velocity. Note that the product of *h* and *v* is width specific surface runoff. *P(x)* (m s^{-1}) denotes water input through precipitation. Infiltration *I* (m s^{-1}) depends on both the hydraulic properties of the soils at the experimental sites and number of macropores.

$$\frac{\partial h(x)}{\partial t} = -\nabla(hv) + P(x) - I(x) \qquad \textbf{(A 1)}$$

The Manning-Strickler formula given in Eq. (A 2). Here surface elevation is denoted by *z* (m) and hydraulic radius, which is the contact area between the flow and the hillslope and denoted by *R* (m). The Strickler coefficient k_{ST} ($m^{1/3}$ s^{-1}) is a measure of roughness showing how much resistance the surface applies to flowing water.

$$v(x) = k_{ST} R^{2/3} \sqrt{2g \frac{d(h+z)}{dx}} \qquad \textbf{(A 2)}$$

https://doi.org/10.5194/egusphere-2026-4957
Preprint. Discussion started: 1 October 2026
© Author(s) 2026. CC BY 4.0 License.

Figure 3 illustrates the open-book framework for both domains, defining the trapezoidal rill width B_r (m), hillslope width B_{HS} (m), downslope length L_{HS} (m), and flow path length L_{FC} (m) where water accumulates. Spatially distributed sheet flow Q_{SF} and rill flow Q_{RF} ($m^3\ s^{-1}$) represent discharge rates driven by rainfall proportional to the projected area along each domain's flow path, with a connection Q_{link} established via the flow accumulation coefficient c_{FC} (-) as formulated in Eq. (A 3). This linkage is governed by the angle γ (rad) between the sheet and rill flow vectors as seen in Eq. (A 4), reflecting whether surface water flows directly down the primary hillslope gradient α (rad) or follows the secondary flow accumulation gradient β (rad) at any given point (Schroers, Eiff et al., 2022).

$$dQ_{link}(x) = Q_{SF}(x) * c_{FC} \quad \textbf{(A 3)}$$

$$\tan(\gamma) = \frac{|\overrightarrow{Q_{RF}}|}{|\overrightarrow{Q_{SF}}|} = \frac{\alpha}{\beta} \quad \textbf{(A 4)}$$

Detachment of particles:

Foster (1982) introduced a relationship to quantify detachment by flow, where the detachment rate is proportional to the shear stress above the erosion resistance of soil. This relationship was later extended by Scherer et al. (2012) to incorporate both the shear stress exerted by overland flow and the rainfall momentum flux acting on the soil surface. Rainfall contributes mass, momentum and kinetic energy to the flow system along the hillslope. While a substantial proportion of the surface runoff kinetic energy dissipates through frictional losses due to surface roughness, the remaining flow energy contributes to the shear stresses driving sediment detachment and transport (Figure 1). Since only the component of rainfall momentum that is perpendicular to the soil surface induces particle detachment, the cosines of the drop angle α_D (°) given in Eq. (A 5) is considered for the calculations of momentum flux m_r ($N\ m^{-2}$), where ρ_w ($kg\ m^{-3}$) is density of water, r ($mm\ h^{-1}$) is precipitation intensity and SC (%) is the soil vegetation cover (Schramm 1994, Bradford and Foster 1996). The formulation of the mean raindrop-fall velocity v_r ($m\ s^{-1}$) is given in Eq. (A 6). In this approach, equal mobilization of all grain-sizes in loess soils is assumed (Scherer 2008).

$$m_r = \rho_w . r . \cos\alpha_D . v_r . (1 - SC) \quad \textbf{(A 5)}$$

$$v_r = 4.459 + 0.613 \ln(r . \cos\alpha) \quad \textbf{(A 6)}$$

$$e_{pot} = p1 . (\tau + p2 . m_r - f_{crit}) \quad \textbf{(A 7)}$$

The relation of the rate of detached soil material to the attacking forces of rainfall and overland flow is described by Eq. (A *7*) in Catflow (Scherer et al. 2012), where τ ($N\ m^{-2}$) is the shear stress exerted by the overland flow on the soil surface. The empirical constants p1 and p2 (-) were derived from controlled experiments as detailed in Scherer et al. (2012) and are representative for the loess soils in the Kraichgau areas. f_{crit} ($N\ m^{-2}$) is the erosion resistance, which is the counteracting force to the shear stress.

Transport of particles:

The sediment transport capacity in the model is computed following the total-load formulation of Engelund and Hansen (1967), which relates sediment transport to flow intensity through transport intensity and bed shear. With this approach, transport of sediments is treated as an energy-driven process and the total transport capacity is estimated from hydraulic variables such as flow velocity, grain-size and density difference between sediment and water. For loess soils, transport capacity is assumed to be non-selective at the bulk scale; fractional sediment loads are assigned by shear-controlled transport capacity and partitioning according to grain-size composition of the soil surface and the transported material. The total amount of sediment in the flow is limited by a defined maximum concentration, ensuring realistic transport rates within the model (Scherer 2008, Schroers et al. 2023).

https://doi.org/10.5194/egusphere-2026-4957
Preprint. Discussion started: 1 October 2026
© Author(s) 2026. CC BY 4.0 License.

Deposition of particles:

Deposition of particles is a size-selective process governed by particle settling velocity and shear stress. Coarse particles settle earlier due to higher sinking velocities, whereas fine particles remain in suspension and are transported over longer distances (Colby 1963). In the model, the net deposition rate is calculated from deposition coefficients, defined for each particle class. These deposition coefficients are derived from the settling velocity of each class, which is computed using the Stokes approach because the particle sizes considered here are very small and the corresponding particle Reynolds numbers fall within the Stokes regime, where viscous forces dominate (Clift et al. 1978, Bird et al. 2002).

Figures

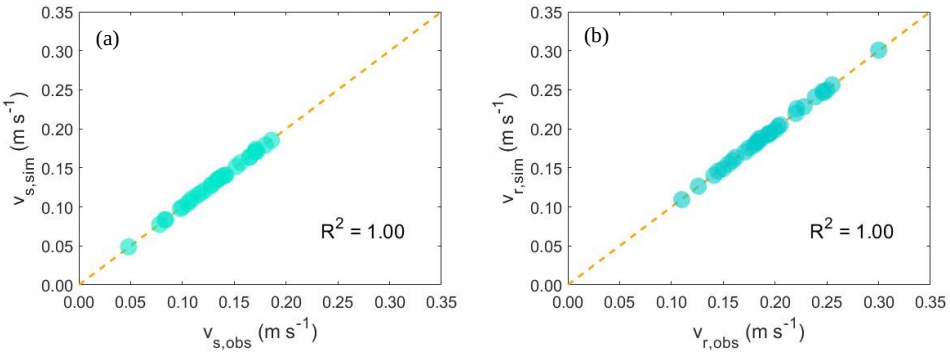

Figure A 1 Simulated vs. observed (a) sheet flow velocity and (b) rill flow velocity for 30 calibrated experiments. The dashed line represents the x=y line.

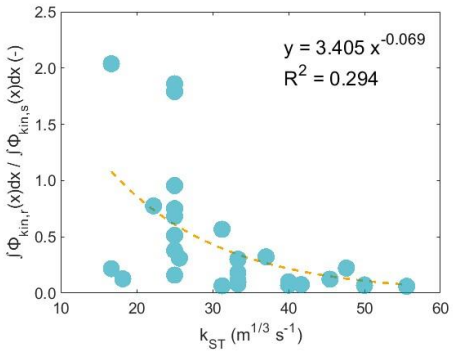

Figure A 2 The ratio of over time integrated kinetic energy flux in the rill domain to that of sheet domain vs. experimental Strickler roughness values (exponential fit) for 30 calibrated experiments.

Tables

Table A 1 Multivariate regression analysis results for all experiments: The F-test probability value represents the overall model significance, and t-test p-values represent the significance of individual parameters.

Function	Number of observations	R^2	Probability value (f-test)	Individual p-values (t-test)	
				θ	k_{ST}
RC=0.045+0.016θ+0.005k_{ST}	60	0.471	1.286*10^{-8}	3.210*10^{-7}	5.252*10^{-5}

https://doi.org/10.5194/egusphere-2026-4957
Preprint. Discussion started: 1 October 2026
© Author(s) 2026. CC BY 4.0 License.

Table A 2 VAN GENUCHTEN-MUALEM parameters (arithmetic mean and standard deviation) for the soil horizons in Weiherbach area (Scherer 2008).

Soil type (horizon)	k_s inverse (m s^{-1})	Θ_s (m^3 m^{-3})	Θ_r (m^3 m^{-3})	α (m^{-1})	n (-)	γ (-)
Pararendzina (Ap horizon)	1.114E-06 ± 1.106E-05	0.440 ± 0.029	0.049 ± 0.033	1.62 ± 1.05	1.296 ± 0.110	0.74 ± 0.86
Loess colluvium (Ap, M horizon)	1.096E-06 ± 8.584E-06	0.441 ± 0.031	0.055 ± 0.035	2.03 ± 1.18	1.170 ± 0.065	0.48 ± 0.67
Keuper colluvium (Ap, M horizon)	1.848E-06 ± 1.182E-05	0.420 ± 0.026	0.106 ± 0.054	10.56 ± 4.00	1.166 ± 0.048	0.41 ± 0.20
Paleosol (Ap, fBt horizon)	1.643E-06 ± 6.133E-06	0.416 ± 0.053	0.118 ± 0.040	7.02 ± 3.85	1.187 ± 0.065	0.48 ± 0.05
Parabraunerde (Ap, Bt horizon)	2.569E-07 ± 8.804E-06	0.460 ± 0.011	0.013 ± 0.005	0.60 ± 0.24	1.339 ± 0.113	0.95 ± 0.83
Parabraunerde (Al horizon)	1.210E-06 ± 3.018E-06	0.450 ± 0.001	0.028 ± 0.020	0.60 ± 0.10	1.654 ± 0.156	1.53 ± 0.61
All soil types (C horizon)	6.803E-07 ± 9.654E-06	0.444 ± 0.033	0.066 ± 0.035	0.51 ± 0.17	2.240 ± 0.449	0.71 ± 0.64

https://doi.org/10.5194/egusphere-2026-4957
Preprint. Discussion started: 1 October 2026
© Author(s) 2026. CC BY 4.0 License.

Table A 3 Soil and runoff characteristics of the 30 experimental setups with model parameters.

	Experimental measurements															Model parameters					
Exp. No.	**Duration (s)**	**Slope (%)**	**Organic matter (%)**	**Precipitation intensity (mm h-1)**	**Clay (%)**	**Fine silt (%)**	**Medium silt (%)**	**Coarse silt (%)**	**Fine sand (%)**	**Medium sand (%)**	**Coarse sand (%)**	$v_{s,obs}$ (m s^{-1})	$v_{r,obs}$ (m s^{-1})	$Q_{cum,obs}$	$S_{cum,obs}$	k_{STr} (m$^{1/3}$ s^{-1})	k_{STs} (m$^{1/3}$ s^{-1})	cf (-)	f_{mak} (-)	f_{crit} (N m^{-2})	Θ_i (%)
1	3600	0,138	1,8	62,4	22,5	7,4	21,1	4,5	3,5	1,5	0,5	0,152	0,246	0,911	84,2	37	41	0,010	1,4	0,710	0,0
2	3540	0,172	1,8	62,4	27,6	7,1	20	40,4	3,3	1,2	0,4	0,171	0,221	0,742	74,7	45,5	45,5	0,007	1,8	0,650	0,0
3	3540	0,117	1,8	62,4	23,5	7,3	21,2	42,5	3,8	1,3	0,4	0,165	0,247	0,805	82,0	47,6	50	0,007	1,8	0,460	0,0
4	2940	0,121	1,8	62,4	21,3	6,7	22,2	43,5	4,1	1,6	0,6	0,156	0,175	0,745	63,2	44	44	0,003	1,1	0,570	0,0
5	3180	0,163	1,7	62,4	15,2	5,2	24,9	48,1	3,7	2,4	0,5	0,133	0,3	1,033	109,2	25	42	0,025	1,0	0,000	0,0
6	3300	0,163	1,9	62,4	16,8	5,3	23,4	48,4	4,3	1,4	0,4	0,122	0,239	0,987	70,2	23	28	0,017	1,1	1,200	0,0
7	4800	0,094	2,5	60,3	25,3	6,2	20,5	44,2	2,8	0,8	0,2	0,18	0,183	1,027	27,5	54	60	0,002	1,5	0,773	0,0
8	4680	0,139	2,5	63,3	28,6	7,8	21,2	39,9	1,9	0,5	0,1	0,118	0,2	0,882	53,0	25	29	0,011	4,3	1,100	0,0
9	7500	0,137	2,0	34,4	30,1	5	20,9	40,4	2,6	0,8	0,2	0,115	0,141	0,620	12,7	25	41	0,009	3,0	0,760	0,0
10	4800	0,137	2,0	62,4	30,1	5	20,9	40,4	2,6	0,8	0,2	0,141	0,195	0,864	42,5	32	38	0,008	4,9	0,970	0,0
11	5880	0,137	2,0	44,6	30,1	5	20,9	40,4	2,6	0,8	0,2	0,1	0,159	0,611	22,4	25	29	0,010	3,4	0,950	0,0
12	4800	0,151	2,5	62,4	21,1	7,3	22,2	44,8	3,1	1,1	0,4	0,142	0,15	1,053	139,3	32	33	0,003	2,0	0,750	0,0
13	5100	0,157	2,2	60,6	26,6	6	21,5	42,7	2,6	0,5	0,1	0,084	0,126	0,475	8,8	17,5	17,5	0,009	5,0	1,720	0,0
14	5100	0,143	1,8	60,6	27,4	5,6	22,6	41	2,6	0,6	0,2	0,128	0,155	0,614	24,0	32	33	0,005	3,2	1,098	0,0
15	5160	0,143	1,6	60,6	27,2	6	21,5	42,1	2,5	0,6	0,1	0,083	0,11	0,437	10,8	18,2	18,2	0,006	5,2	1,540	0,0
16	4320	0,147	2,2	60,6	21,8	6,2	21,9	45,1	3,6	0,9	0,5	0,17	0,187	0,622	32,3	50	49	0,003	2,2	0,855	15,0
17	4339,8	0,147	1,6	60,6	20,6	5,5	23,5	45,1	3,9	1,1	0,3	0,128	0,145	0,458	15,7	34	34	0,004	3,8	1,060	13,0
18	4260	0,146	1,7	60,6	18,9	6,2	23,8	45,3	4,2	1,1	0,5	0,11	0,22	0,642	42,5	25	30	0,015	2,0	0,910	15,0
19	5460	0,144	2,0	60,6	24,3	7,6	22,2	42,7	2,5	0,5	0,2	0,105	0,205	0,619	21,6	25,5	29	0,014	4,8	1,030	13,0
20	4860	0,132	1,6	60,6	24,1	7	22,4	42,7	3	0,6	0,2	0,078	0,185	0,438	16,3	16,7	24	0,020	4,5	0,950	12,0
21	4860	0,132	1,6	60,6	24,4	7,6	21,2	43	3	0,6	0,2	0,107	0,25	0,593	25,9	25	39	0,020	4,0	0,705	14,0
22	4080	0,149	1,4	63	18,7	5,9	23,4	47	3,7	0,9	0,4	0,098	0,18	0,302	19,1	24	27	0,013	5,5	0,945	12,0
23	4080	0,149	1,6	59,9	17,8	5,9	23,1	48,1	3,9	0,9	0,3	0,186	0,194	0,457	29,4	51	65	0,005	3,8	0,550	13,0
24	5049,6	0,179	1,6	60,6	17,1	7,5	23,9	46,3	3	1,3	0,9	0,048	0,162	0,617	81,6	25	5	0,009	3,0	1,027	14,0
25	4500	0,178	1,6	60,6	16,8	5,8	24,8	46,4	4,2	1,3	0,7	0,135	0,255	0,746	115,8	31,3	35	0,016	1,8	0,746	15,0
26	4500	0,178	1,6	62,3	16,8	5,8	24,8	46,4	4,2	1,3	0,7	0,139	0,228	0,666	45,8	34	35	0,012	2,8	1,020	14,0
27	5280	0,182	1,5	59,2	12,7	5,1	24,1	51,1	4,8	1,4	0,8	0,172	0,203	0,882	182,9	40	45	0,007	2,0	0,552	15,0
28	4200	0,148	1,6	64,8	17,3	5,3	21,5	49,5	4,5	1,3	0,6	0,135	0,171	0,614	61,9	33,3	35	0,006	3,5	0,850	14,0
29	3720	0,150	1,3	62,4	15,6	5,4	23,9	47,3	4,1	3,2	0,5	0,17	0,182	1,051	134,4	39	43	0,004	1,3	0,620	0,0
30	3840	0,168	1,1	62,4	16,6	6,1	20,4	41,9	7,9	5	2,1	0,165	0,193	0,995	114,7	39	39	0,005	1,6	0,750	0,0

https://doi.org/10.5194/egusphere-2026-4957
Preprint. Discussion started: 1 October 2026
© Author(s) 2026. CC BY 4.0 License.

Code and data availability

The model parameterization and experimental data are provided in the appendix. Further observational data and the model code are available from the corresponding author upon reasonable request.

Author contributions

DY designed the methodology, expanded the open book approach, performed the modelling, formal analysis and data visualization, and wrote the original draft of the manuscript. SS provided the theoretical groundwork, suggested the open book approach, and contributed to the review and editing of the manuscript. US carried out model development and the groundwork for the model setups, and contributed to the review and editing of the manuscript. NMC contributed to the review and editing of the manuscript. EZ contributed to the conceptualization, supervision, and review and editing of the manuscript.

Competing interests

At least one of the (co-)authors is a member of the editorial board of Hydrology and Earth System Sciences.

Acknowledgements

The authors gratefully acknowledge the Weiherbach Project for providing the experimental data used in this study. The contribution of the project to advancing research on rainfall-runoff responses and their modelling is sincerely appreciated.

Financial support

This research was funded in whole, or in part, by the Luxembourg National Research Fund (FNR) and the Ministry of Agriculture, Food and Viticulture (MAAV), grant reference 17965325. For the purpose of open access, and in fulfilment of the obligations arising from the grant agreement, the author has applied a Creative Commons Attribution 4.0 International (CC BY 4.0) license to any Author Accepted Manuscript version arising from this submission.

References

Abrahams, A. D., et al. (1986). "Resistance to overland flow on desert hillslopes." Journal of Hydrology **88**: 343-363.

Abrahams, A. D., et al. (1994). "Resistance to overland flow on semiarid grassland and shrubland hillslopes, Walnut Gulch, southern Arizona." Journal of Hydrology **156**(1): 431-446.

Ahmad, P. I. D. M. F., et al. (2011). "The Critical Shear Stresses for Sand and Mud Mixture." Applied Mathematical Sciences **5**.

Bagnold, R. A. (1966). "An approach to the sediment transport problem." US Geological Survey Professional Paper **422-I**.

Bennett, J. P. (1974). "Concepts of Mathematical Modeling of Sediment Yield." Water Resources Research **10**(3): 485-492.

Bergkamp, G. (1998). "A hierarchical view of the interactions of runoff and infiltration with vegetation and microtopography in semiarid shrublands." Catena **33**: 201-220.

Beven, K. and P. Germann (1982). "Macropores and water flow in soils." Water Resources Research **18**: 1311-1325.

Bird, R. B., et al. (2002). Transport Phenomena. New York, John Wiley & Sons.

Bradford, J. M. and G. R. Foster (1996). "Interrill Soil Erosion and Slope Steepness Factors." Soil Science Society of America Journal **60**(3): 909-915.

Cammeraat, E. L. H. (2004). "Scale dependent thresholds in hydrological and erosion response of a semi-arid catchment in southeast Spain." Agriculture, Ecosystems & Environment **104**(2): 317-332.

https://doi.org/10.5194/egusphere-2026-4957
Preprint. Discussion started: 1 October 2026
© Author(s) 2026. CC BY 4.0 License.

Clift, R., et al. (1978). Bubbles, Drops, and Particles. New York, Academic Press.

Colby, B. (1963). Fluvial sediments a summary of source, transportation, deposition, and measurement of sediment discharge. Bulletin.

Collier, N., et al. (2011). "Diffusive Wave Approximation to the Shallow Water Equations: Computational Approach." Procedia Computer Science **4**: 1828-1833.

Darboux, F., et al. (2002). "Evolution of overland flow pathways in rough surfaces." Water Resources Research **38**.

Dingman, S. L. (2015). Physical Hydrology. Long Grove, Illinois, Waveland Press, Inc.

Dunne, T., et al. (1991). "Effects of rainfall, vegetation, and microtopography." Water Resources Research **27**: 2271-2285.

Emmet, W. W. (1978). "Overland Flow." Hillslope Hydrology: 145-176.

Engelund, F. and E. Hansen (1967). A monograph on sediment transport in alluvial streams. Copenhagen.

Engman, E. T. (1986). "Roughness Coefficients for Routing Surface Runoff." Journal of Irrigation and Drainage Engineering **112**(1): 39-53.

Foltz, R., et al. (2008). "Modeling changes in rill erosion and critical shear stress on native-surface roads." Hydrological Processes **22**.

Foster, G. R. (1982). Modeling the erosion process. Hydrologic Modeling of Small Watersheds. C. T. Haan, H. P. Johnson and D. L. Brakensiek. St. Joseph, Michigan, USA, American Society of Agricultural Engineers**:** 297-380.

Gerlinger, K. (1997). Erosionsprozesse auf Lößböden: Experimente und Modellierung.

Gilley, J. E., et al. (1993). "Critical Shear Stress and Critical Flow Rates for Initiation of Rilling." Journal of Hydrology **142**.

Giménez, R. and G. Govers (2001). "Interaction between bed roughness and flow hydraulics." Water Resources Research **37**: 791-799.

Goodrich, D. C., et al. (1995). "Measurement and Analysis of Small-Scale Convective Storm Rainfall Variability." Journal of Hydrology **173**(1-4): 283-308.

Govers, G., et al. (2007). "Rill erosion: Exploring the relationship between experiments, modelling and field observations." Earth-Science Reviews **84**(3): 87-102.

Govers, G., et al. (2000). "Soil roughness and overland flow." Agronomie **20**(2): 131-146.

Govers, G., et al. (2007). "Soil erosion and flow concentration." Earth Surface Processes and Landforms **32**: 591-608.

Gupta, H. V., et al. (1998). "Toward improved calibration of hydrologic models." Water Resources Research **34**: 751-763.

He, S., et al. (2024). "Response of Hydrodynamic Characteristics to Tillage-Induced Microtopography of Rill Erosion Processes under Heavy Rainfalls." Land **13**(5): 685.

Hergarten, S. (2020). "Energy-based models of geomorphic systems." Earth Surface Dynamics **8**: 1041-1060.

Horton, R. E. (1945). "Erosional Development of Streams and Their Drainage Basins - Hydrophysical Approach to Quantitative Morphology." Geological Society of America Bulletin **56**(3): 275-370.

Kampf, S. K. and B. B. Mirus (2013). "Treatise on Geomorphology: 9.3 Subsurface and Surface Flow Leading to Channel Initiation." Elsevier **9**: 22-42.

Klaus, J. and E. Zehe (2011). "A novel explicit approach to model bromide and pesticide transport in connected soil structures." Hydrol. Earth Syst. Sci. **15**(7): 2127-2144.

Kleidon, A., et al. (2013). "Thermodynamics, maximum power, and the dynamics of preferential river flow structures at the continental scale." Hydrology and Earth System Sciences **17**(1): 225-251.

Knapen, A., et al. (2007). "Resistance of soils to concentrated flow erosion: A review." Earth-Science Reviews **80**(1): 75-109.

Lesschen, J. P., et al. (2009). "Modelling runoff and erosion for a semi-arid catchment using a multi-scale approach based on hydrological connectivity." Geomorphology **109**(3): 174-183.

Li, D., et al. (2024). "Response of erosion rate to hydrodynamic parameters in sheet and rill erosion process on saturated soil slopes." Soil and Tillage Research **237**: 105996.

https://doi.org/10.5194/egusphere-2026-4957
Preprint. Discussion started: 1 October 2026
© Author(s) 2026. CC BY 4.0 License.

Loritz, R., et al. (2017). "Picturing and modeling catchments by representative hillslopes." Hydrology and Earth System Sciences **21**(2): 1225-1249.

Martinkova, M. and J. Kysely (2020) "Overview of Observed Clausius-Clapeyron Scaling of Extreme Precipitation in Midlatitudes." Atmosphere **11**, 786 DOI: 10.3390/atmos11080786.

Maurer, T. (1997). Physikalisch begründete, zeitkontinuierliche Modellierung des Wassertransports in kleinen ländlichen Einzugsgebieten.

Meyer-Peter, E. and R. Müller (1948). "Formulas for bed-load transport." Proceedings IAHR.

Molnar, P., et al. (2015). "Storm type effects on super Clausius–Clapeyron scaling of intense rainstorm properties with air temperature." Hydrol. Earth Syst. Sci. **19**(4): 1753-1766.

Nearing, M. A., et al. (1997). "Hydraulics and erosion in overland flow." Soil Science Society of America Journal **61**: 1419-1426.

Nearing, M. A., et al. (1997). "Hydraulics and erosion in eroding rills." Water Resources Research **33**(4): 865-876.

Nearing, M. A., et al. (2004). "Expected climate change impacts on soil erosion rates: A review." Journal of Soil and Water Conservation **59**(1): 43-50.

Niu, Y., et al. (2025). "Spatiotemporal variations of the rill morphology and hydraulic characteristic on spoil heaps." Journal of Soils and Sediments **25**: 3134-3148.

Penna, D., et al. (2011). "The influence of soil moisture on runoff generation." Hydrology and Earth System Sciences **15**: 1927-1941.

Peters, A. (2014). "Simple consistent models for water retention and hydraulic conductivity in the complete moisture range." Water Resources Research **49**(10): 6765-6780.

Poesen, J., et al. (2003). "Gully erosion and environmental change: importance and research needs." CATENA **50**(2): 91-133.

Puigdefabregas, J., et al. (1999). "Scales and processes of water and sediment redistribution in drylands: results from the Rambla Honda field site in Southeast Spain." Earth-Science Reviews **48**(1-2): 39-70.

Reaney, S. M., et al. (2014). "Connectivity in hydrological systems." Earth Surface Processes and Landforms **39**: 159-172.

Richet, J.-B., et al. (2017). "The role of vegetative barriers such as fascines and dense shrub hedges in catchment management to reduce runoff and erosion effects: Experimental evidence of efficiency, and conditions of use." Ecological Engineering **103**: 455-469.

Scherer, U. (2008). Prozessbasierte Modellierung der Bodenerosion in einer Lösslandschaft.

Scherer, U., et al. (2012). "Prediction of soil detachment in agricultural loess catchments: Model development and parameterisation." Catena **90**: 63-75.

Schramm, M. (1994). An erosion model with spatially and temporally variable rill morphology. Communications from the Institute for Hydraulic Engineering and Agricultural Engineering at the University of Karlsruhe. Karlsruhe, Germany, University of Karlsruhe.

Schroers, S., et al. (2022). "Morphological controls on Hortonian surface runoff: An interpretation of steady-state energy patterns, maximum power states and dissipation regimes within a thermodynamic framework." Hydrology and Earth System Sciences: 3125-3150.

Schroers, S., et al. (2023). "Energy efficiency in transient surface runoff and sediment fluxes on hillslopes – a concept to quantify the effectiveness of extreme events." Hydrology and Earth System Sciences **27**: 2535-2557.

Seibert, S., et al. (2011). "Surface runoff from arable land - a homogenized data base of 762 rainfall simulation experiments, CRC/TR32 Database (TR32DB)."

Takken, I., et al. (1998). "Effects of tillage-induced roughness." Water Resources Research **34**: 2279-2289.

Trenberth, K., et al. (2003). "The Changing Character of Precipitation." Bulletin of the American Meteorological Society **84**: 1205-1218.

https://doi.org/10.5194/egusphere-2026-4957
Preprint. Discussion started: 1 October 2026
© Author(s) 2026. CC BY 4.0 License.

Vrugt, J. A., et al. (2003). "A shuffled complex evolution approach." Water Resources Research **39**.

Wainwright, J. and A. J. Parsons (2002). "The effect of temporal variations in rainfall on scale dependency in runoff coefficients." Water Resources Research **38**: 1271.

Wainwright, J., et al. (2011). "Linking environmental régimes, space and time: Interpretations of structural and functional connectivity." Geomorphology **126**(3): 387-404.

Western, A. W., et al. (2002). "Scaling of soil moisture: A hydrologic perspective." Annual Review of Earth and Planetary Sciences **30**: 149-180.

Winterwerp, J., et al. (2012). "A conceptual framework for shear flow-induced erosion of soft cohesive sediment beds." Journal of Geophysical Research (Oceans) **117**: 10020.

Wooding, R. A. (1965). "A hydraulic model for the catchment-stream problem." Journal of Hydrology **3**: 254-267.

Xinlan, L., et al. (2015). "The effect of different soil erosion stages on surface roughness under simulated rainfall." Nature Environment and Pollution Technology **14**: 9-16.

Zehe, E. (1999). Stofftransport in der ungesättigten Bodenzone auf verschiedenen Skalen.

Zehe, E., et al. (2005). "Uncertainty of simulated catchment runoff response in the presence of threshold processes: Role of initial soil moisture and precipitation." Journal of Hydrology **315**(1-4): 183-202.

Zehe, E. and G. Blöschl (2004). "Predictability of hydrologic response at the plot and catchment scales: Role of initial conditions." Water Resources Research **40**(10).

Zehe, E., et al. (2001). "Modeling water flow and mass transport in a loess catchment." Physics and Chemistry of the Earth Part B-Hydrology Oceans and Atmosphere **26**(7-8): 487-507.

Zhang, G.-h., et al. (2009). "Sediment Transport and Soil Detachment on Steep Slopes: I. Transport Capacity Estimation." Soil Science Society of America Journal **73**(4): 1291-1297.

Zhao, L., et al. (2014). "Soil surface roughness change and its effect on runoff and erosion on the Loess Plateau of China." Journal of Arid Land **6**(4): 400-409.